# Supporting Information

## Miceli et al. 10.1073/pnas.1216867110

### SI Results

**Modeling the Effects of R213W and R213Q $K_V7.2$ Mutations on Neuronal Excitability in Heteromeric Conditions only with $K_V7.2$ Subunits.** Although it is widely believed that M-current ($I_{KM}$) is formed from a 2+2 combination of $K_v7.2$ and $K_v7.3$ subunits at most neuronal sites, $K_v7.2$ subunit expression is observed in the absence of $K_v7.3$ in Ranvier nodes in central and peripheral fibers (1, 2) and, possibly, presynaptic nerve terminals (3). $K_v7.2$ homomers also provide a major contribution to $I_{KM}$ at early developmental stages of rat superior cervical ganglion neurons (4). To investigate the effects of the R213Q and R213W mutant subunits when incorporated at a 2:2 ratio with $K_v7.2$ subunits, we performed modeling experiments under conditions in which somatic and axonal $I_{KM}$ incorporated the kinetic and steady-state parameters experimentally derived from homomeric $K_V7.2$ channels, and from $K_v7.2$/$K_v7.2$ R213W and $K_v7.2$/$K_v7.2$ R213Q heteromers (namely, in the absence of $K_v7.3$ at both somatic and axonal compartments; Fig. S1). Compared with $K_v7.2$/$K_v7.3$ heteromers, currents carried by $K_v7.2$ homomers display similar kinetics, but activate at slightly more depolarized potentials (Table 1) (5). As a consequence, using in our CA1 model an $I_{KM}$ with kinetics and steady-state properties of $K_v7.2$ homomers resulted in a lower activation of $I_{KM}$ around the resting potential (compare Fig. S1*B* with Fig. 4*B*). This in turn caused the neuron to become slightly more excitable, as revealed by the higher spike number elicited across a wide range of injected current (compare Fig. S1*C* with Fig. 4*C*) and peak $I_{KM}$ conductances (compare Fig. S1*D* with Fig. 4*D*). More importantly, also under these experimental conditions, a strong increase in cell excitability was observed in $K_v7.2$/$K_v7.2$ R213W and $K_v7.2$/$K_v7.2$ R213Q heteromers, with the latter showing more dramatic effects.

**Modeling the Effects of R213W and R213Q $K_V7.2$ Mutations on Neuronal Excitability in Heteromeric Conditions with $K_V7.2$ Subunits (Axon) and with $K_V7.2$ and $K_V7.3$ Subunits (Soma).** In the simulations shown in Fig. 4 and in Fig. S1, a threefold larger density within the axonal vs. the somatic compartment was used for $I_{KM}$ to take into account the polarized expression of $K_v7.2/3$ subunits. To evaluate the effects of a differential expression of $K_v7.2$ and $K_v7.3$ subunits at distinct subcellular sites, we carried out simulations in which experimental data for $K_v7.2$/Kv7.3 heteromers were included to model the somatic component of $I_{KM}$, whereas data for $K_v7.2$ homomers were used to model the axonal $I_{KM}$ (Fig. S2). The results obtained suggested that, under this condition, neurons carrying WT subunits can exhibit an excitability profile [action potential (AP) number as a function of injected currents and $I_{KM}$ conductance] intermediate between those of Fig. 4 (in which $K_v7.2$/$K_v7.3$ heteromeric channels have been modeled at somatic an axonal locations) and Fig. S1 (in which $K_v7.2$ homomers are present in soma and axons). More importantly for our purposes, use of R213W and R213Q mutant $K_v7.2$ channels caused an increased intrinsic excitability of the model neuron. As in Fig. 4 and in Fig. S1, this increase appears consistently more dramatic for the R213Q than for the R213W mutation.

**Modeling Effects of $K_v7.2$ R213W and R213Q Mutations on Neuronal Bursting Behavior.** As previously described (6), the present computational model was originally developed to provide insights into the experimental results showing that blocking $K_v7$ channels with XE-991 did not produce bursting activity, but rather spontaneous sustained firing. On the contrary, Yue and Yaari (7) showed that blockade of $I_{KM}$ with linopirdine for 15 to 20 min depolarized the neurons by approximately 5 mV, and converted single spike responses evoked by brief depolarizing currents to a burst of few (on average, three) spikes. Longer drug exposure also led to the appearance of spontaneous unprovoked firing, similarly to the results of Shah et al. (6). To investigate the effects of the R213Q and R213W mutations in $K_v7.2$ on bursting behavior, we first modified the original model in such a way that (using WT $K_v7.2$ subunits always in heteromeric configuration with $K_v7.3$ as in Fig. 4), $I_{KM}$ blockade generated a self-limiting burst of few spikes (Fig. S3, *Top*). This was obtained by mainly increasing the $I_{KM}$ and $Ca^{2+}$-dependent conductances (8). Next, we made a reasonable estimate of the resting membrane potential in neurons carrying the R213W and R213Q mutations (which is currently unavailable from experiments). By looking at the resting values of the activation for each case, we assumed that R213Q-carrying neurons would be slightly depolarized (~3 mV), whereas R213W-carrying neurons would have a resting membrane potential value very similar to that of WT neurons. The model predicts that, under these conditions, in contrast with the self-limiting burst of few spikes observed in WT neurons, in neurons carrying R213W or R213Q subunits, $I_{KM}$ blockade will generate a long-lasting bursting behavior, with a higher spike number for R213Q- than for R213W-carrying neurons. These data thus suggest that both mutations would increase bursting behavior, with stronger effects prompted by the R213Q compared with the R213W mutation.

**Effect of Replacement of F at Position 168 with Nonaromatic Residue on Gating Properties of $K_v7.2$, $K_v7.2$ R213Q, and $K_v7.2$ R213W Channels.** To validate our structural assumption that the R213W mutation causes less dramatic functional consequences on channel gating compared with the R213Q mutation in $K_v7.2$ by creating a π-stacking interaction with the neighbor F168 residue in S3, the aromatic F168 residue was replaced with a leucine (F168L), a nonpolar amino acid. This specific substitution was chosen because the closely related subunit $K_v7.3$ carries an L at the corresponding position (see alignment in Fig. S4), thereby minimizing the potential risk of expressing nonfunctional, lethal subunits. As a matter of fact, homomeric channels formed by $K_v7.2$ subunits carrying the F168L mutation were functional when expressed in CHO cells (Fig. S4), and carried currents with biophysical properties only slightly different from those of WT channels. Compared with WT $K_v7.2$ channels, $K_v7.2$ F168L channels displayed a 7 mV more depolarized midpoint potential of activation, together with a slightly decreased slope of the normalized current–voltage curve (Fig. S5) and slower deactivation time constants (Fig. S6).

To investigate the differential interaction of the F168 residue with the Q or the W at position 213, the F168L mutation was also incorporated in subunits carrying the R213Q or R213W mutations, thus generating the F168L-R213W and F168L-R213Q double mutants. Homomeric $K_v7.2$ channels carrying F168L-R213W and F168L-R213Q subunits were fully functional (Fig. S4), and generated currents whose gating properties were dominated by the lack of the positive charge at R213. In fact, currents carried by both F168L-R213W and F168L-R213Q channels displayed a markedly depolarized midpoint potential of activation (Fig. S5), together with significantly faster deactivation kinetics (Fig. S6). Following channel opening, $K_v7.2$ channels carrying F168L-R213W and F168L-R213Q subunits almost completely deactivated after pulses to −20 mV of 1.5 seconds duration (Fig. S6). More importantly, the gating differences between channels carrying R213Q and R213W subunits were

largely reduced in F168L-R213Q and F168L-R213W double mutants. In fact, no differences were observed in midpoint potential of the normalized current–voltage curve (Fig. S5), as well as in deactivation kinetics and extent, between homomeric channels carrying the F168L-R213Q and F168L-R213W double mutations (Fig. S6); by contrast, a significant difference in the slope of the normalized current–voltage curve still persisted when comparing homomeric channels formed by $K_v$7.2 F168L-R213Q and F168L-R213W subunits, with the latter channels, similarly to R213W singly mutated channels, showing a less steep normalized current–voltage relationship (Fig. S5).

These results provide experimental support to the hypothesis that the F at position 168 is critical to confer a lesser degree of gating impairment to the R213W mutation compared with the R21Q mutation. We thus speculate that the π-stacking interaction between the W213 and the F168 is therefore crucial to mitigate the gating disruption caused by the mutation-induced removal of the positive charge at position R213.


1. Devaux JJ, Kleopa KA, Cooper EC, Scherer SS (2004) KCNQ2 is a nodal K+ channel. *J Neurosci* 24(5):1236–1244.
2. Schwarz JR, et al. (2006) KCNQ channels mediate IKs, a slow K+ current regulating excitability in the rat node of Ranvier. *J Physiol* 573(pt 1):17–34.
3. Martire M, et al. (2004) M channels containing KCNQ2 subunits modulate norepinephrine, aspartate, and GABA release from hippocampal nerve terminals. *J Neurosci* 24(3):592–597.
4. Hadley JK, et al. (2003) Stoichiometry of expressed KCNQ2/KCNQ3 potassium channels and subunit composition of native ganglionic M channels deduced from block by tetraethylammonium. *J Neurosci* 23(12):5012–5019.
5. Soldovieri MV, et al. (2006) Decreased subunit stability as a novel mechanism for potassium current impairment by a KCNQ2 C terminus mutation causing benign familial neonatal convulsions. *J Biol Chem* 281(1):418–428.
6. Shah MM, Migliore M, Valencia I, Cooper EC, Brown DA (2008) Functional significance of axonal Kv7 channels in hippocampal pyramidal neurons. *Proc Natl Acad Sci USA* 105(22):7869–7874.
7. Yue C, Yaari Y (2004) KCNQ/M channels control spike afterdepolarization and burst generation in hippocampal neurons. *J Neurosci* 24(19):4614–4624.
8. Migliore M, Ascoli GA, Jaffe DB (2010) Hippocampal microcircuits. *Springer Series in Computational Neuroscience*, eds Cutsuridis V, Graham B, Cobb S, Vida I (Springer, Heidelberg), Vol 5, pp 353–374.


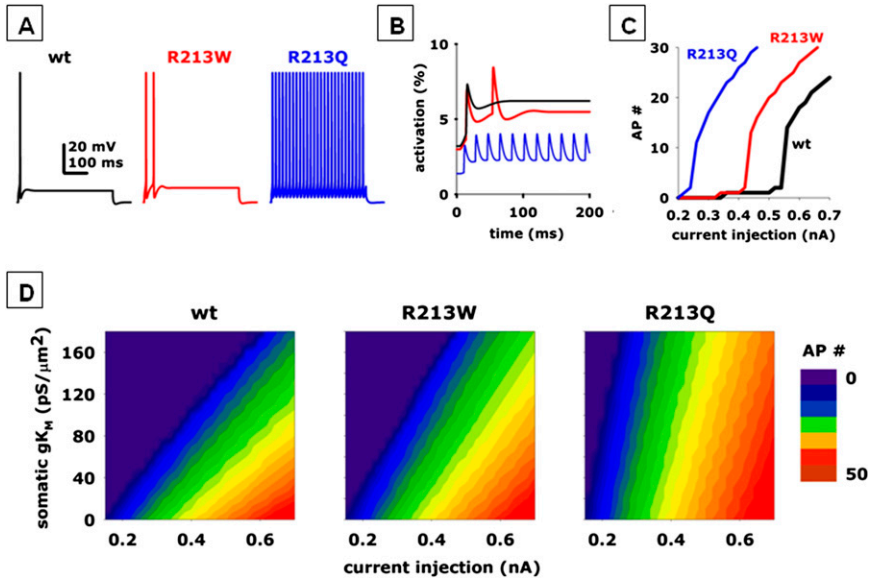


**Fig. S1.** Modeling of the effects of R213W and R213Q $K_V$7.2 mutations on neuronal excitability in heteromeric conditions only with $K_V$7.2 subunits. Time course of the somatic membrane potential (*A*) and $I_{KM}$ currents activation (*B*; only expanded sweeps of the first 200 ms are shown) from CA1 neurons expressing $K_V$7.2 (black traces), $K_V$7.2+$K_V$7.2 R213W (red traces), or $K_V$7.2+$K_V$7.2 R213Q (blue traces) heteromeric channels, during a 500-ms somatic current injection of 0.65 nA. (*C*) Input/output (I/O) curves from cells expressing $K_V$7.2 (black trace), $K_V$7.2+$K_V$7.2 R213W (red trace), or $K_V$7.2+$K_V$7.2 R213Q (blue trace) heteromeric channels. Number of APs (AP#) is expressed as a function of the somatic current injected, using a 120 mS/μm$^2$ peak $I_{KM}$ conductance. (*D*) Contour plots for number of APs elicited by a 500-ms somatic current injection from cells expressing $K_V$7.2, $K_V$7.2+$K_V$7.2 R213W, or $K_V$7.2+$K_V$7.2 R213Q heteromeric channels as a function of current injection and peak $I_{KM}$ conductance.

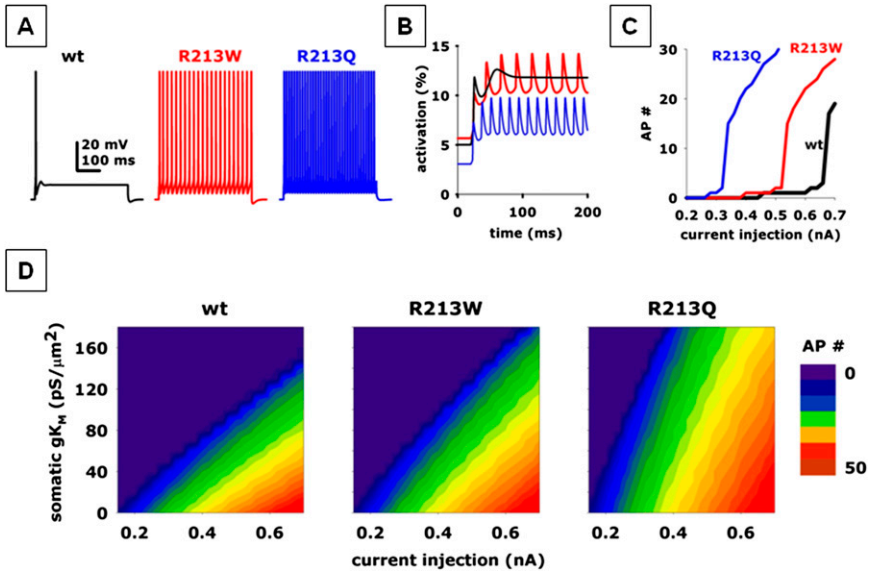


**Fig. S2.** Modeling of the effects of R213W and R213Q $K_V7.2$ mutations on neuronal excitability in heteromeric conditions with $K_V7.2$ subunits (axon) and with $K_V7.2$ and $K_V7.3$ subunits (soma). Time course of the somatic membrane potential (*A*) and $I_{KM}$ currents activation (*B*; only expanded sweeps of the first 200 ms are shown) from CA1 neurons expressing $K_V7.2$+$K_V7.3$ (black traces), $K_V7.2$+$K_V7.2$ R213W+$K_V7.3$ (red traces), or $K_V7.2$+$K_V7.2$ R213Q+$K_V7.3$ (blue traces) heteromeric channels in the soma, and $K_V7.2$ (black traces), $K_V7.2$+$K_V7.2$ R213W (red traces), or $K_V7.2$+$K_V7.2$ R213Q (blue traces) heteromeric channels in the axon, during a 500-ms somatic current injection of 0.65 nA. (*C*) Input/output (I/O) curves. Number of APs (AP#) is expressed as a function of the somatic current injected, using a 120-mS/μm$^2$ peak $I_{KM}$ conductance. (*D*) Contour plots for number of APs as a function of current injection and peak $I_{KM}$ conductance.

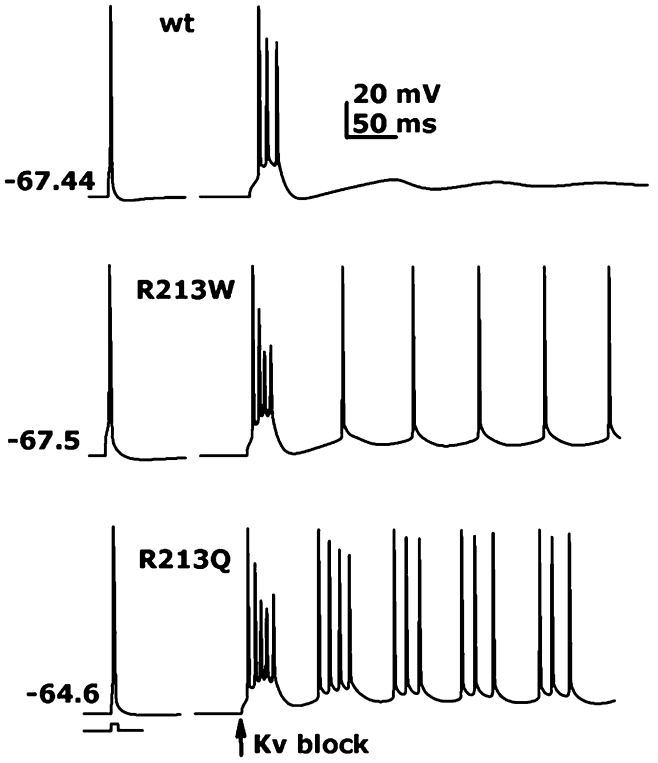


**Fig. S3.** Modeling of the effects of the $K_V7.2$ R213W and R213Q mutations on neuronal bursting behavior. Time course of the somatic membrane potential from simulations of a CA1 neuron expressing $K_V7.2$+$K_V7.3$ (*Top*), $K_V7.2$+$K_V7.2$ R213W+$K_V7.3$ (*Middle*), or $K_V7.2$+$K_V7.2$ R213Q+$K_V7.3$ (*Bottom*) heteromeric channels. A single test action potential was first elicited with a short somatic current pulse under control conditions. At 600 ms, $I_{KM}$ was blocked (arrow, Kv block). This caused different spontaneous bursting behavior under each condition.

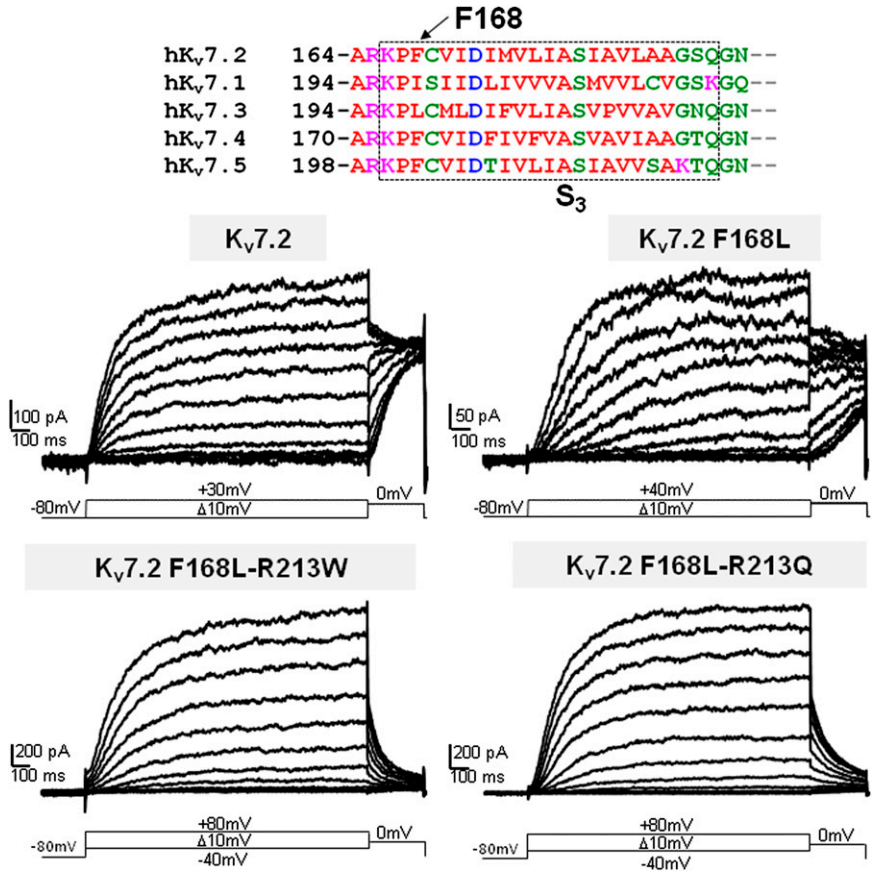


**Fig. S4.** Functional properties of homomeric $K_v7.2$ channels carrying F168L, F168L+R213W, and F168+R213Q subunits. (*Upper panel*) Sequence alignment of the S3 segments of the indicated $K_v7$ subunits (www.ebi.ac.uk/Tools/psa/). Residues are colored according to the following scheme: magenta, basic; blue, acid; red, nonpolar; and green, polar. Note that the F residue at position 168 in $K_v7.2$ is also present in $K_v7.4$ and $K_v7.5$ subunits. (*Lower panels*) Macroscopic current traces from CHO cells expressing $K_v7.2$, $K_v7.2$ F168L, $K_v7.2$ F168L-R6W, and $K_v7.2$ F168L-R6Q channels, in response to the indicated voltage protocols. Current scale, 100 pA; time scale, 0.1 s.

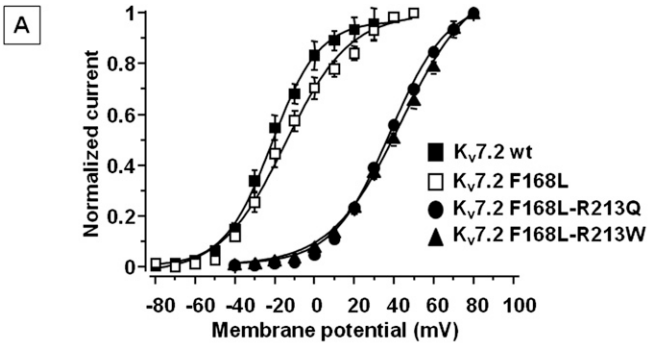


B

| | n | $V_{½}$ (mV) | *k* (mV/e-fold) |
|---|---|---|---|
| $K_v7.2$ | 17 | -22.2±0.7 | 12.2±0.7 |
| $K_v7.2$ F168L | 6 | -14.1±4.4† | 16.6±1.3† |
| $K_v7.2$ F168L-R213W | 4 | 43.6±3† | 18.2±1†,§ |
| $K_v7.2$ F168L-R213Q | 10 | 39.1±1.3† | 15.5±0.8† |

p<0.05 vs the corresponding value in: †$K_v7.2$, and §$K_v7.2$ F168L-R213Q.

**Fig. S5.** Steady-state gating properties of $K_v7.2$ channels carrying F168L, F168L+R213W, and F168+R213Q subunits. (*A*) Conductance/voltage curves for the indicated channels. Continuous lines are Boltzmann fits to the experimental data. (*B*) $V_{1/2}$ and *k* values obtained from the Boltzmann fits for the indicated channels.

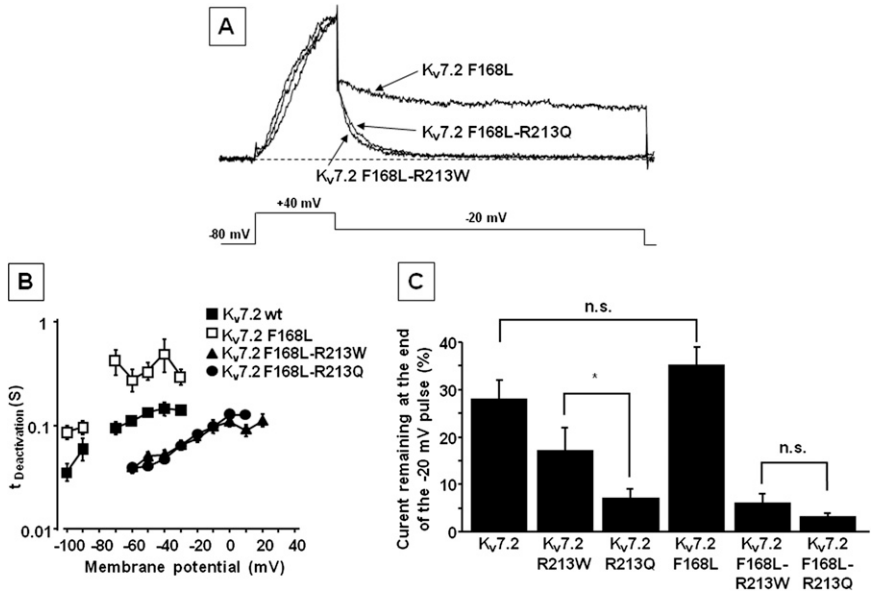


**Fig. S6.** Gating kinetics of $K_v$7.2 channels carrying F168L, F168L+R213W, and F168+R213Q subunits. (*A*) Normalized and superimposed current traces from $K_v$7.2 F168L, F168L+R213W, and F168+R213Q channels, in response to the indicated voltage protocol. (*B*) Time constants for ionic current deactivation for the indicated channels. (*C*) Plot of the current remaining at the end of the deactivating −20 mV pulse, following the protocol shown in *B*, for the indicated channels. $*P < 0.05$; n.s., not significantly different.